3D.6 ESTIMATES OF HURRICANE WIND SPEED MEASUREMENT ACCURACY USING THE AIRBORNE HURRICANE IMAGING RADIOMETER

Ruba A. Amarin*, Linwood Jones[1], James Johnson[1], Christopher Ruf[2], Timothy Miller[3] and Shuyi Chen[4]

[*1] Central Florida Remote Sensing Laboratory
University of Central Florida, Orlando, Florida 32816, U.S.A
* ramarin@mail.ucf.edu
[2] Space Physics Research Laboratory, University of Michigan, Ann Arbor, Michigan
[3] NASA Marshall Space Flight Center, Huntsville, Alabama
[4] University of Miami, Miami, Florida

ABSTRACT

This paper presents results from research conducted at the Central Florida Remote Sensing Laboratory, to estimate the HIRAD wind speed and rain rate measurement performance in hurricanes under realistic operating conditions. These computer simulations use the MM5 numerical hurricane model as the "nature run" to provide realistic 3D environmental parameters (rain, water vapor, clouds and surface winds) from which wide-swath brightness temperature measurements are calculated using an advanced radiative transfer model (RTM). This RTM includes a rain model for the hurricane environment and an ocean surface emissivity model for hurricane force winds over incidence angles from nadir to > 60°. Simulations were done for typical high altitude "Figure-4" flight tracks on a global Hawk unmanned aircraft, and include realistic sources of errors, such as antenna pattern and cross-polarization effects, which are expected in the actual observations.

Using these simulated HIRAD measurements with errors, Monte Carlo retrievals of wind speed and rain rate were performed using databases of sea surface temperatures and climatological hurricane atmospheric parameters. Examples of retrieved hurricane wind speed and rain rate images are presented, and comparisons of these retrieved parameters with the nature run are made. Statistical analyses are performed and RMS measurement errors are characterized over a broad range of wind and rain conditions and as a function of path length over the full HIRAD swath. These results will be used as error estimates for HIRAD performance in future numerical Observing System Simulation Experiments (OSSEs).

1. INTRODUCTION

The measurement of peak winds in hurricanes is critical to classification of hurricane intensity. The Hurricane Imaging Radiometer (HIRAD) is an airborne passive microwave remote sensor that has been developed to retrieve ocean surface wind speed and rain rate within tropical cyclones through category-5 intensities. HIRAD is a multi-frequency microwave radiometer at C-band that is based on the existing technique of the C-band Stepped Frequency Microwave Radiometer (SFMR), Uhlhorn (2007), which operates from NOAA and Air Force reconnaissance aircraft to measure along track surface winds and rain rate. HIRAD adds the capability for cross-track observations by using synthetic thinned array radiometry technology, resulting in 2 – 5 km cross-track resolution over a swath width of approximately 70 km, when operating from a high-altitude aircraft (60,000 feet) above the storm and provides real aperture imaging along track, Tanner and Swift (1993). This technology is currently under development at the NASA Marshall Space Flight Center in a collaborative effort with NOAA Hurricane Research Division, the Central Florida Remote Sensing Laboratory (CFRSL) at the University of Central Florida (UCF) and the University of Michigan.

* *Corresponding author address:* Ruba A. Amarin, Univ. of Central Florida, Orlando, FL 32828; e-mail: ramarin@mail.ucf.edu

This paper deals with the remote sensing of wind speed and rain rate in hurricanes, which directly supports the HIRAD instrument development. Through the use of realistic simulations of hurricane surveillance flights over ocean, we are able to predict the wind speed measurement performance of a conceptual pushbroom wide-band radiometer system that has strong similarities with HIRAD. The goal of this research is to use this simulation to characterize the HIRAD hurricane surface wind speed measurement accuracy as a function of wind speed, rain rate and cross-swath location (earth incidence angle, EIA). We use proven methods of microwave radiometer measurement modeling in a Monte Carlo simulation to predict wind speed retrieval errors parametrically with instrument characteristics, and the results of the simulation are directly applicable to the HIRAD performance.

2. HIRAD EQUIVALENT PUSHBROOM RADIOMETER SYSTEM

In this paper, results are presented for a simulated real aperture pushbroom radiometer equivalent of HIRAD, which is shown in Fig. 1. In the simplest terms, the equivalent system replaces the HIRAD synthetic thinned array imaging with 41 individual antenna beams (with boresight spaced on 3° centers ±60°). These beams are contiguous at nadir and they overlap at the edges of the swath.

The pushbroom antenna beams were implemented as 4 different antenna designs (one per frequency) that are scanning phased arrays that produce similar patterns to the synthesized beams for HIRAD. Thus, the pushbroom patterns are equivalent in terms of the C-band operating frequencies, approximate antenna pattern spatial resolutions, cross-track boresight pointing angles (every 3°) and polarization. The HIRAD antenna is designed to measure the horizontally polarized brightness temperature emission from the surface over ±60° in the cross-track direction.

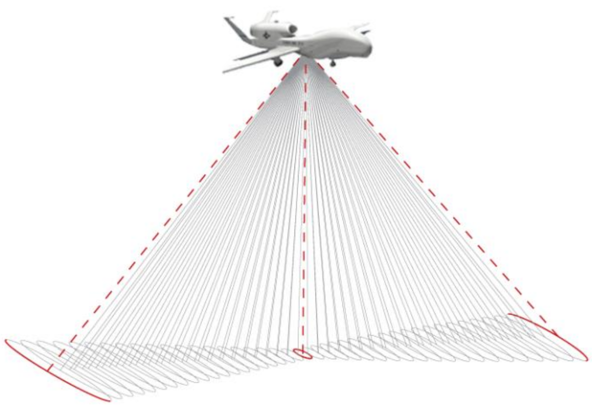

Figure 1 Equivalent real-aperture radiometer system with 41 beams cross-track.

3. HURRICANE FORWARD RADIATIVE TRANSFER MODEL

As part of the HIRAD development, the CFRSL radiative transfer model, RTM, was tuned for hurricane environment. The selected approach was to use the SFMR rain algorithm, which is derived from the work of Jorgensen and Willis (1982) and Olsen et al. (1978), and to develop an improved microwave radiometric ocean surface emissivity model, El-Nimri et al. (2010).

3.1 Atmosphere Forward Model

The RTM, Hong (2008), has 39 atmospheric layers of 20 km total thickness, which are used to compute the water vapor, cloud liquid water and oxygen absorption coefficients. For the HIRAD frequencies, only water vapor and cloud liquid absorption in hurricanes are significant.

The MM5 hurricane "nature run" simulations were from a state-of-art numerical model described by Chen et al. (2007). A model run for Hurricane Frances (2004) provides realistic 3D environmental parameters (rain, water vapor, clouds and surface winds) from which simulated HIRAD T_b's are derived for typical aircraft "Fig-4" flight tracks. The MM5 model uses a system of nested grids with the innermost one having a horizontal grid spacing of 0.015 degrees (~1.6 km resolution) in longitude and latitude.

In the forward radiative transfer model, each simulated HIRAD measurement (cross-track pixel) will have a unique surface wind speed and atmospheric profile, which uses a mesh grid criterion by dividing the atmosphere into 39 layers and the ground into 1.67 km pixels (corresponding to the MM5 resolution). This procedure approximates the actual HIRAD T_b measurement whereby the upwelling and downwelling T_b components to be calculated along different slant paths. The pushbroom antenna boresight geometry calculations are performed based on the HIRAD antenna sampling for the cross-track scans.

3.2 Antenna Brightness Temperature

The simulation uses a real aperture phased array antenna to produce multiple antenna beams in a pushbroom configuration for the wide-swath surface sampling, which is approximately equivalent to the HIRAD brightness temperature image synthesis. The HIRAD measurement is horizontal (H-Pol) but the cross-polarization (V-Pol) must also be included. Therefore, both the H-Pol and V-Pol scene apparent T_b are computed from the forward model and are convolved with the co-polarized (Co-Pol) and cross-polarized (X-Pol) antenna patterns respectively. The resulted convolved H-Pol and V-Pol temperatures are given by Ulaby (1981),

$$T_{bHconv} = \frac{\int_0^{2\pi}\int_{-\theta}^{\theta} T_{ap\,h}(\theta,\Phi)\times F_{Co-Pol}(\theta,\Phi)\times sin\theta d\ \theta \mathrm{d}\Phi}{\int_0^{2\pi}\int_{-\theta}^{\theta} F_{Co-Pol}(\theta,\Phi)\times sin\theta d\ \theta \mathrm{d}\Phi} \qquad (1)$$

$$T_{bVconv} = \frac{\int_0^{2\pi}\int_{-\theta}^{\theta} T_{apv}(\theta,\Phi)\times F_{X-Pol}(\theta,\Phi)\times sin\theta d\ \theta \mathrm{d}\Phi}{\int_0^{2\pi}\int_{-\theta}^{\theta} F_{X-Pol}(\theta,\Phi)\times sin\theta d\ \theta \mathrm{d}\Phi} \qquad (2)$$

In (1), the horizontally convolved T_b is integrated over $\pm\theta_1 = \pm 30°$ that results in ~ 100% beam efficiency for the Co-Pol antenna pattern, whereas in the vertically convolved T_b given by (2), the θ limits change by beam position to insure > 90% beam efficiency.

The final convolved brightness temperature, T_A, is a superposition of T_{bHconv} and T_{bVconv} according to,

$$T_A = (1-\gamma)T_{bH_{conv}} + \gamma T_{bVconv} \qquad (3)$$

where γ is the ratio of the X-Pol brightness temperature to the total and is approximated by,

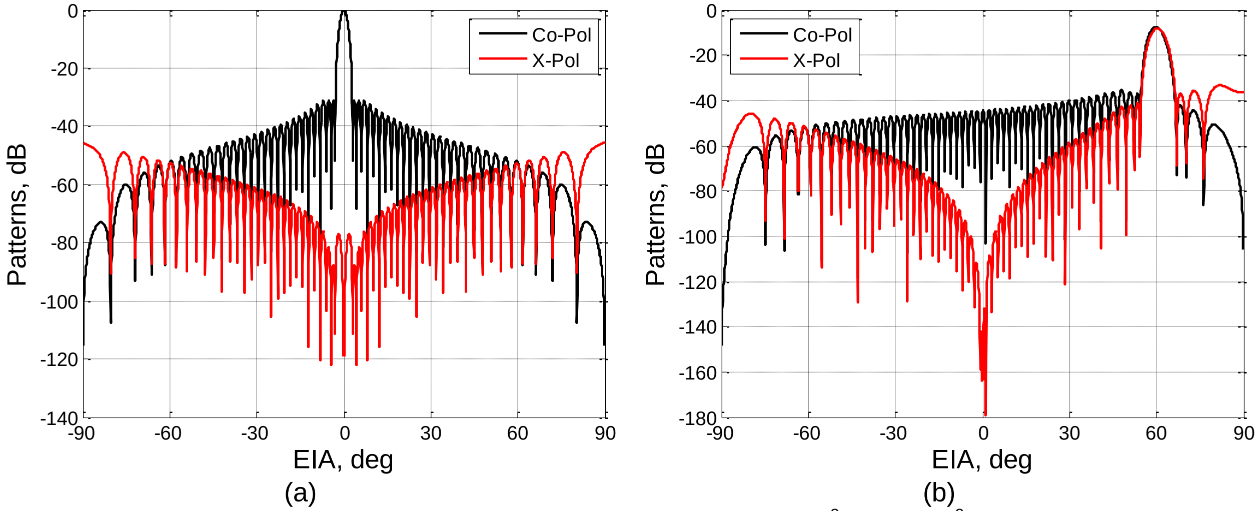

Figure 2 Co-Pol and X-Pol patterns at 6.6 GHz frequency for (a) 0^o and (b) 60^o scan beams.

$$\gamma = \frac{\int_{FirstNulls} XPol}{\int_{FirstNulls} XPol + \int_{FirstNulls} CoPol} \quad (4)$$

γ changes as a function of incidence angle (beam position) for each frequency and increases with angles; for the nadir beam (Fig. 2(a)), nearly all the brightness is from Co-Pol making γ approximately equal to zero. On the other hand, for the beam position at 60^o (Fig. 2(b)), where both patterns have the same power gain, results in approximately half of the measured brightness coming from X-Pol and half from the Co-Pol, making $\gamma \sim 0.5$.

4. GEOPHYSICAL RETRIEVAL ALGORITHM

A retrieval algorithm known as the Hurricane Imaging Retrieval Algorithm was developed for rain rate and wind speed retrievals in hurricanes. It is composed of a forward radiative transfer model and an inversion algorithm.

4.1 Atmospheric Treatment

The retrieval algorithm RTM is slightly different than the forward RTM model used in the simulation. First, the hurricane climatology atmosphere vertical profiles used in the retrievals vary radially with distance from the eye. This is in contrast with the simulated forward model, where the atmosphere varies both horizontally and vertically in a 3D sense as described earlier in Section 3.1. Further, there is a major difference in the treatment of rain; where the height of the rain is fixed at a constant freezing level of 5 km in the retrievals whereas for the forward RTM, the rain height from the hurricane numerical weather model varies and the upwelling and downwelling T_b components are calculated along different slant paths. Also for the retrieval RTM, the sea surface temperature is assumed to be a constant value of 28 deg Celsius in comparison to the actual SST image used in the forward simulation.

To calculate the atmospheric absorption coefficients, a priori hurricane climatology environmental parameters were developed using the 3D atmosphere generated from the hurricane MM5 model. The atmospheric data (temperature, water vapor density and cloud liquid) were averaged in the 39 layers over radial annuli of 5 km increments. Each annulus was assigned the mean value of the vertical profile and the resultant water vapor and cloud liquid water absorption coefficient profiles are in Np/km. The sum of these absorption coefficients along with an additional absorption coefficient due to rain is used in the computation of the modeled brightness temperature (T_{mod}) at each of the four C-band frequencies. These T_b's are placed into a three dimensional matrix for each frequency with wind speed, rain rate and angles as variables.

4.2 Antenna Pattern Correction

In order to correct for the antenna pattern convolution effect in the retrieval algorithm, the V-Pol effect was removed from the total antenna brightness temperature (T_A) computation according to,

$$T_{bHconv} = \frac{T_A - \gamma \times T_{bVconv}}{(1-\gamma)} \quad (5)$$

The V-Pol convolved temperatures, T_{bVconv}, in (5) are estimated based on the best linear fit relationships with the convolved brightness temperature, T_A.

After solving for T_{bHconv}, the T_b due to the antenna pattern was corrected for as shown in (6),

$$T_{Corr} = \frac{1}{\eta_{ML}}[T_{bHconv} - \eta_U \times T_U - \eta_B \times T_B] \qquad (6)$$

where T_U and T_B are the brightness temperatures that correspond to the "above the boresight" and "below the boresight" portions of the pattern. These T_b's are computed as part of the simulated forward model based on the best linear fit relationships with T_A.

η_{ML}, η_U, and η_B are the correspondent beam efficiencies of the main lobe, above and below the boresight respectively.

4.3 Retrieval Algorithm

There are three main sources of errors that have been modeled in the retrieval module and those include the instrument T_b errors which involves the NEDT and the ΔG/G, the aircraft attitude and the geophysical model function (emissivity model) errors. In the simplest terms, these errors are modeled as random errors that have probability distribution functions that are zero mean Gaussian with a STD that was varied parametrically for 1, 2, 4 and 8 Kelvin cases.

The modeled brightness temperature matrix, T_{mod}, is compared to the corrected brightness temperature with random errors added, (T_{corr} + *Noise*), at each of the four frequencies. Each element in the difference matrices is squared and the algorithm searches for the minimum of the summed squared difference surface, over all frequencies. This process is repeated 50 times in a Monte-Carlo simulation for each beam position and scan to collect RMSE statistics.

5. RESULTS

Comprehensive simulations for assessing HIRAD performance were conducted and three Fig-4 patterns were simulated, with 6 flight legs 30^o apart and two legs outside the eye to capture high rain bands at relatively low wind speed values. Each flight leg is made up of 240 individual HIRAD scans, resulting in a total of 1920 scans over the HIRAD swath for the eight legs. The MM5 modeled data, serving as surface truth, is compared to the retrieved wind speed values and RMS wind speed errors are computed from the differences. Figure 3 shows the surface truth wind speed (m/s) and integrated rain rate (km-mm/hr) for two Frances legs along with the RMS retrieved wind speed errors (m/s) for 1 Kelvin random error. The highest errors are associated with larger incidence angles and with rain bands. We see higher wind speed errors at the edges of the swath where X-Pol effect is high, path lengths are greatest and rain is the most intense since we are still in the eye wall region. Heavy rain, even in the inner swath, can cause relatively high wind speed errors.

Retrieved wind speed and rain rate error statistics for all noise levels in the parametric error analysis are summarized in Table 1. The mean error in retrieved wind speed is approximately 1 m/s or less for simulated measurement errors up to 4 Kelvin, and the STD of the error follows the 1 m/s per Kelvin rule. The mean integrated rain rate error corresponds to an average over the path of a few mm/hr or less, depending on location in the swath. However, there are significant rain rate errors at higher rain rates and in some cases at the swath edges.

TABLE I

ERROR STATISTICS FOR ALL CASES

Noise Added (Kelvin)	**0**	**1**	**2**	**4**	**8**
Wind Speed Mean (m/s)	-0.27	-0.35	-0.58	-1.17	-2.62
Wind Speed STD (m/s)	0.99	1.51	2.48	4.55	8.21
Rain Rate Mean (km.mm/hr)	10.36	10.55	11.32	13.50	22.39
Rain Rate STD (km.mm/hr)	29.24	31.45	37.66	55.16	95.56

Results from eight flight legs for the 1 Kelvin error case are shown in Fig. 4 where retrieved wind speed and integrated rain rate are compared to the surface truth values. The color-bar on the wind speed comparison refers to integrated rain rate values in km-mm/hr. Relatively large errors in retrievals occur in the low wind speed region due to the nature of the surface GMF at relatively low wind speeds, where emissivity is highly sensitive to wind speed. Otherwise the wind speed agreement looks good over the entire swath, even where heavy rain exists. The retrieved rain rate, on the other hand, is over estimated at higher rain rate values, which is correlated with longer slant paths (edges of swath) and the difference in the rain modeling in the forward RTM (representing the measurement) and the retrieval RTM.

6. SUMMARY & CONCLUSION

HIRAD simulation for wide swath microwave brightness temperature observations of a hurricane and retrieval algorithms for surface wind speed and rain rate have been developed. Nature run using the MM5 numerical model for wind and rain fields for hurricane Frances, 2004 were used in estimating HIRAD wind speed retrieval errors. Retrieval algorithm was based on the HIRAD geometry, and an equivalent HIRAD antenna design. Realistic aircraft surveillance flight patterns through Frances were simulated, including instrument errors. The retrieved wind field compares well to the surface truth over most of the swath, but antenna pattern effects along with differences in the atmosphere treatment caused some large wind speed errors near ± 60^o in the presence of intense rain.

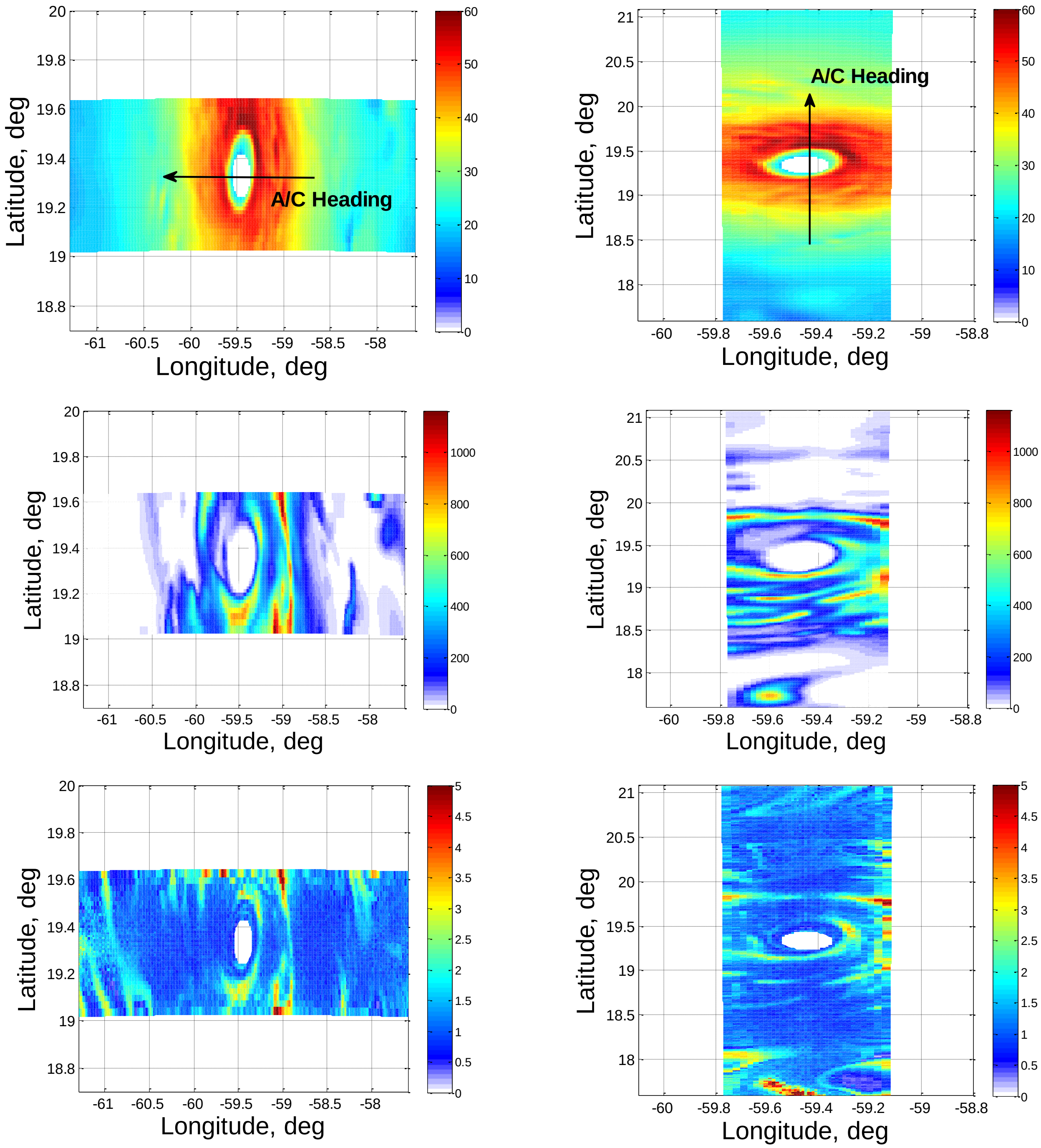

(a) (b)

Figure 3 Surface truth wind speed (m/s) and integrated rain rate (km-mm/hr) along with the RMS retrieved wind speed errors (m/s) for 1 Kelvin random error for (a) leg 1 and (b) leg 2.

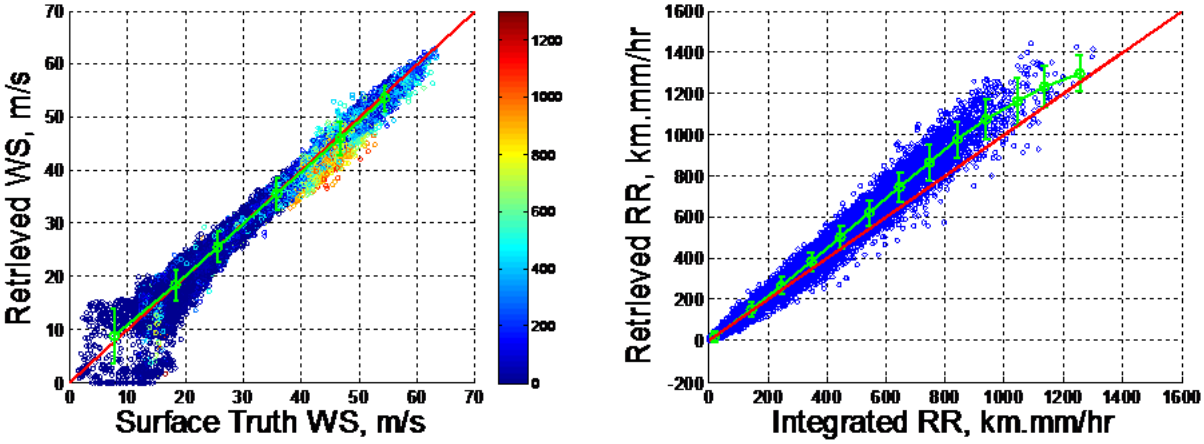

(a) (b)

Figure 4 Scatter plot comparisons for (a) wind speed and (b) rain rate for eight legs.

7. REFERENCES

Uhlhorn, E. W., Black, P. G., Franklin, J. L., Goodberlet, M., Carswell, J., Goldstein, A. S., 2007: Hurricane surface wind measurements from an operational stepped frequency microwave radiometer. *American Meteorological Society*.

Tanner, A. B. and Swift, C. T., 1993: Calibration of a synthetic aperture radiometer. *IEEE Trans. Geosci. Remote Sensing*, vol. 31, pp. 257-267.

Jorgensen, D. P. and Willis, P. T., 1982: A Z-R relationship for hurricanes. *Journal of Applied Meteorology*, vol. 21, pp. 356-366.

Olsen, R. L., Rogers, D. V. and Hodge, D. B., 1978: The aR^b relation in the calculation of rain attenuation. *IEEE Trans. Antennas Propagat.*, vol. 26, pp. 318-329.

El-Nimri, S. F., Jones, W. L., Uhlhorn, E., Ruf, C., Johnson, J., and Black, P., 2010: An improved C-band ocean surface emissivity model at hurricane-force wind speeds over a wide range of earth incidence angles. *IEEE Geoscience and Remote Sensing Letters*.

Hong, L., 2008: Inter-satellite microwave radiometer calibration. Ph.D. Dissertation, University of Central Florida, School of EECS.

Chen, S. S., Price, J. F., Zhao, W., Donelan, M. A., Walsh, E. J., 2007: The CBLAST-hurricane program and the next-generation fully coupled atmosphere-wave-ocean models for hurricane research and prediction. *Bull. Amer. Meteor. Soc.*, 88(3), 311-317.

Ulaby, F. T., Moore, R. K. M., and Fung, A. K. 1981: Microwave remote sensing, active and passive. vol. 1. Chapter 4, Section 4.5, pp. 203-208, Norwood, MA: Artech House Inc.